eprints@whiterose.ac.uk
https://eprints.whiterose.ac.uk/

A detailed micro-modelling approach for the structural analysis of masonry assemblages

V. Sarhosis[1][*], J.V. Lemos[2]

[1]School of Engineering, Newcastle University, Newcastle upon Tyne, UK
[2]National Laboratory for Civil Engineering, Lisbon, Portugal

Abstract

Over the last 50 years, a significant amount of effort has been taken to develop numerical approaches and tools for the structural analysis of masonry. These range from considering masonry as an anisotropic continuum (macro-models) to the more detailed ones considering masonry as an assemblage of units and joints (micro-models). In this paper, a detailed micro-modelling approach for the analysis of masonry couplets and prisms is proposed. The approach represents masonry units and mortar joints as an assemblage of densely packed discrete irregular deformable particles bonded together by zero thickness interface laws. The mechanical properties (here referred to as micro-properties) of irregular particles and contacts are responsible for the mechanical behaviour of masonry. In addition, the approach allows failure to occur either at the brick, mortar and/or brick/mortar interface. A series of computational models were developed and their results are compared against small-scale experimental findings. A good agreement between the experimental and the numerical results was obtained which demonstrates the huge potential of the modelling approach proposed. The significant advantage of this approach is to model cracking as a real discontinuity among particles and not as a modification in the material properties. In addition, reliable prediction of masonry strength can allow one to reduce the costly and timely experimental testing and avoid the reliance on conservative empirical formulas.

Highlights

- A detailed micro-modelling approach to represent the micro-structure of masonry assemblages proposed
- Masonry considered as an assemblage of densely packed discrete irregular particles
- A fair to good agreement between the experimental and the numerical results was obtained
- Cracking allowed to occur either at the brick, mortar and/or brick/mortar interface
- Approach can be used as a tool to understanding of the processes related to the brittle failure of masonry.

Corresponding author: Dr Vasilis Sarhosis, School of Engineering, Newcastle University, NE1 3AB, Newcastle Upon Tyne, UK, email: vasilis.sarhosis@newcastle.ac.uk .

List of Abbreviation

A_c — Contact area

σ — Stress

σ_n — Normal stress

K_n — Nodal stiffness

M_n — Nodal mass

$\dot{u}$ — Velocity

x_i — Node coordinates

τ_{fr} — Residual strength

τ_u — Ultimate shear strength

ΔF^n — Normal force increment

ΔF^s — Shear force increment

Δt_n — Limiting time-step

ΔUn — Normal contact displacement increment

ΔUs — Shear contact displacement increment

Δt — Time step

Deg — Degrees

E — Modulus of elasticity

f_t — Tensile strength

Jcoh — Joint cohesion

Jdil — Joint dilation angle

Jfric — Joint friction angle

Jfric_res — Residual joint friction angle

JKn — Joint normal stiffness

JKs — Joint shear stiffness

Jten — Joint tensile strength

OPC	Ordinary Portland Cement
T	Tension
TT	Tensile Test
u	Deformation
Un	Normal contact displacement
Us	Shear contact displacement
v	Poisson coefficient
τ_{max}	Maximum shear stress
τ_{res}	Residual shear strength
τ_s	Shear stress
τ_u	Ultimate shear stress
$F(t)$	Total nodal force
$frac$	User-defined time-step reduction factor
m	Mass
t	Time

1. Introduction

Masonry is a heterogeneous anisotropic material, which is composed of units (e.g. bricks, stones, blocks etc.), bonded together with or without mortar. It is probably the oldest building material that is commonly used today. Although masonry is easy to construct, its mechanical behaviour is non-linear and thus complex to understand. Movements in masonry may arise due to the application of external load, foundation settlement, temperature and moisture variations. Such movements could lead to several different defects in serviceability state such as cracking and ultimate limit state such as crushing and spalling (Hendry 1998). In masonry, cracking can occur: a) at the masonry units; b) at the mortar; c) at the brick/mortar interface; and d) in all of the above. Cracks in masonry may not open uniformly but may close and open according to the type of stresses applied to them over time. Cracking in masonry reduces its load carrying capacity and could lead, eventually, to collapse of the structure.

The need to predict the in-service behaviour and load carrying capacity of masonry has led researchers to develop several computational strategies and tools that are characterized by different levels of complexity. These range from the classical plastic solution methods (Heyman, 1998) to the most advanced non-linear computational formulations (e.g. finite element and discrete element methods of analysis). The selection of the most appropriate method to use depends on, among other factors, the structure under analysis; the level of accuracy and simplicity desired; the knowledge of the input properties in the model and the experimental data available; the amount of financial resources; time requirements and the experience of the modeller (Lourenço, 2002). Also, it should be expected that different methods should lead to different results depending on the adequacy of the approach and the information available. Preferably, the approach selected to model masonry should provide the desired information in a reliable manner within an acceptable degree of accuracy and with least cost.

For a numerical model to adequately represent the behaviour of a real structure, both the constitutive model and the input material properties must be selected carefully by the modeller to take into account the variation of masonry properties and the range of stress state types that exist in masonry structures (Sarhosis et al., 2016a). It is also important that the numerical model is able to capture the failure mechanisms which can occur in masonry. Figure 1 shows five basic failure mechanisms: (a) and (b) are mortar joint mechanisms, (d) is a masonry unit mechanism and (c), (e) are combined mechanisms involving cracking in both units and mortar. However, variation in the stress-state within masonry can lead to combined failure modes in the structure. The occurrence of the mode of failure will depend on the magnitude and direction of the shear and normal stress.
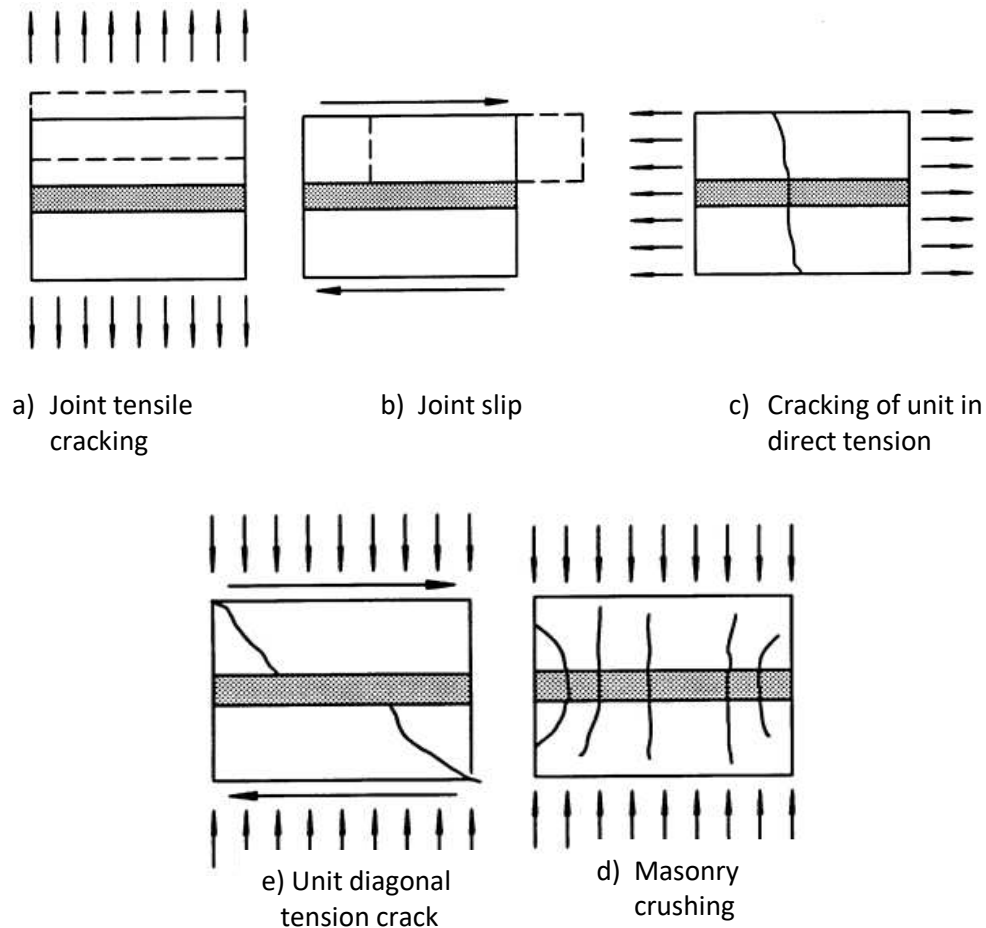
Figure 1. Masonry failure mechanisms (Lourenço and Rots, 1997)

At present, the approaches used to simulate the mechanical behaviour of masonry tend to focus on the individual masonry units and the mortar (i.e. micro-models), or on the composite material (i.e. macro-models). The most commonly used numerical tool for the analysis of masonry structures is the finite element method where masonry units and mortar joints are smeared out in a homogeneous anisotropic continuum (Lourenço, 1996; Lourenço et al., 1998; Pela et al., 2012; Castellazzi et al., 2018). Although, this approach is widely used and is able to simulate large structures, a significant limitation is its inability to model discontinuities between different blocks of the masonry or individual cracks formed in the structure when external load applied to them. To overcome the above limitations, joint interface elements were introduced to model discontinuities in masonry (Lourenço and Rots, 1997; Giambanco et al., 2001). In this case, each mortar joint, consisting of the mortar and the two unit-to-mortar interfaces, is lumped into an "average" interface while the units are slightly expanded in size in order to keep the geometry unchanged. With this approach it is possible to consider masonry as a set of elastic blocks bonded together by potential fracture slip lines at the joints. In this way, cracking can only occur at the interfaces and not in the masonry units. Another restriction is that most of these methods were not able to allow for finite displacement and rotation including complete detachment of blocks. To overcome this limitation, some finite element formulations (Berto et al., 2002; Radnić et al. 2012; Milani & Taliercio 2015 & 2016) as well as other attractive tools, like the discrete element method (Sarhosis et al. 2016b;

Lemos 2007; Smoljanović et al. 2013) have been developed. Such approaches are suitable for modelling the non-linear behaviour of masonry and allow finite sized discrete bodies that can move (and potentially deform) independently to each other; automatic detection and update of new contacts and loss of existing contacts between the elements as the simulation progresses; and large displacements and rotations with complete detachment of blocks. For an exhaustive discussion on the numerical methods available, the reader is referred to (Sarhosis 2016; Roca et al. 2010).

Reducing the amount of interfaces is good (and hence the extreme simplification to reduce mortar to a single interface), although information about the actual crack pattern within the mortar is lost. Detailed micro-modelling is probably the most accurate tool available today to simulate the real behaviour of masonry as the elastic and inelastic properties of both the units and the mortar can be realistically taken into account. Within this method, a suitable constitutive law is introduced in order to reproduce not only the behaviour of the masonry units and mortar, but also their interaction. However, any analysis with this level of refinement requires large computational effort. Thus, this method is mainly used to simulate tests on small specimens in order to determine accurately the stress distribution in the masonry materials. Reliable prediction of masonry strength is of great value for engineers since it allows to reduce the amount of experimental tests to be carried out and avoid the usage of conservative and empirical formulae.

Discrete element models based on bonded circular particles have been used successfully in detailed analysis of laboratory tests on rock specimens (Potyondy and Cundall, 2004). An application of a bonded particle model to the in-plane analysis of a stone masonry wall was presented by Azevedo et al. (2016). More recently, discrete element block models using polygonal particles have been proposed in the field of rock mechanics. While computationally more expensive, they have shown a superior performance in matching the observed rock fracture behaviour (Lan et al., 2010; Kazerani and Zhao, 2010; Cruz and Pierce, 2014). Pina-Henriques & Lourenço (2006) applied a related concept, but using FE models, in a very detailed analysis of brick failure under compressive loads.

In this paper, a phenomenological two dimensional model based on the detailed micro-modelling approach which is able to predict the mechanical (both shear, tension and compression) behaviour of masonry couplets and prisms is proposed. In this modelling approach, the micro-structure of masonry units and mortar are considered as an assemblage of densely packed irregular in shape and size discrete elements bonded together by a zero thickness interface. Such irregular elements could be a few milimiters in size and are able to move independantly to each other and open or slide, thus allowing for cracking in either brick, mortar and/or brick-mortar interface. The previous work in rock mechanics has shown the potential of this conceptual approach, as the random network of potential discontinuities is capable of simulating in a realistic manner the geometric complexity of failure modes in geomaterials. The manuscript is organised as follows. Section 2 presents the main features of the discrete element modelling approach proposed. Section 3 describes the numerical vs. experimental comparisons. Finally, Section 4 outlines the conclusions and major findings of this work.

2. An alternative approach to model fracture in masonry units and mortar using DEM

The proposed model is based on a phenomenological approach which aims to capture the failure mechanisms and quasi-brittle behaviour (i.e. cracking rather than a plastic yield) of masonry. For further information about the quasi-brittle behaviour of masonry the reader is directed to (Hendry 1998; Lourenco 1998; Massart 2003). The proposed model was developed in a discrete element framework, the 2D code UDEC (Itasca, 2014). The key features required to implement the proposed approach are described below.

2.1 Representation of masonry units and mortar

The discontinuous nature of masonry components was considered by giving a fictitious random microstructure to units and mortar. In this way, both masonry units and mortar are composed of continuum elements of polygonal or Voronoi shape (Mayya & Rajan 1994) (hereafter named *inner-blocks*, see Figure 2). Inner-blocks can be subdivided into simple triangular finite elements (designated as zones) (Figure 3), which give a much better approximation of the strain field than an assumption of uniform strain in the whole inner-block. In the present work, the discrete deformable inner-block elements containing internal meshing are assumed elastic, but a non-linear material behaviour may also be used if necessary. Inner blocks can take any arbitrary shape and could be even used to model irregular and rubble masonry.
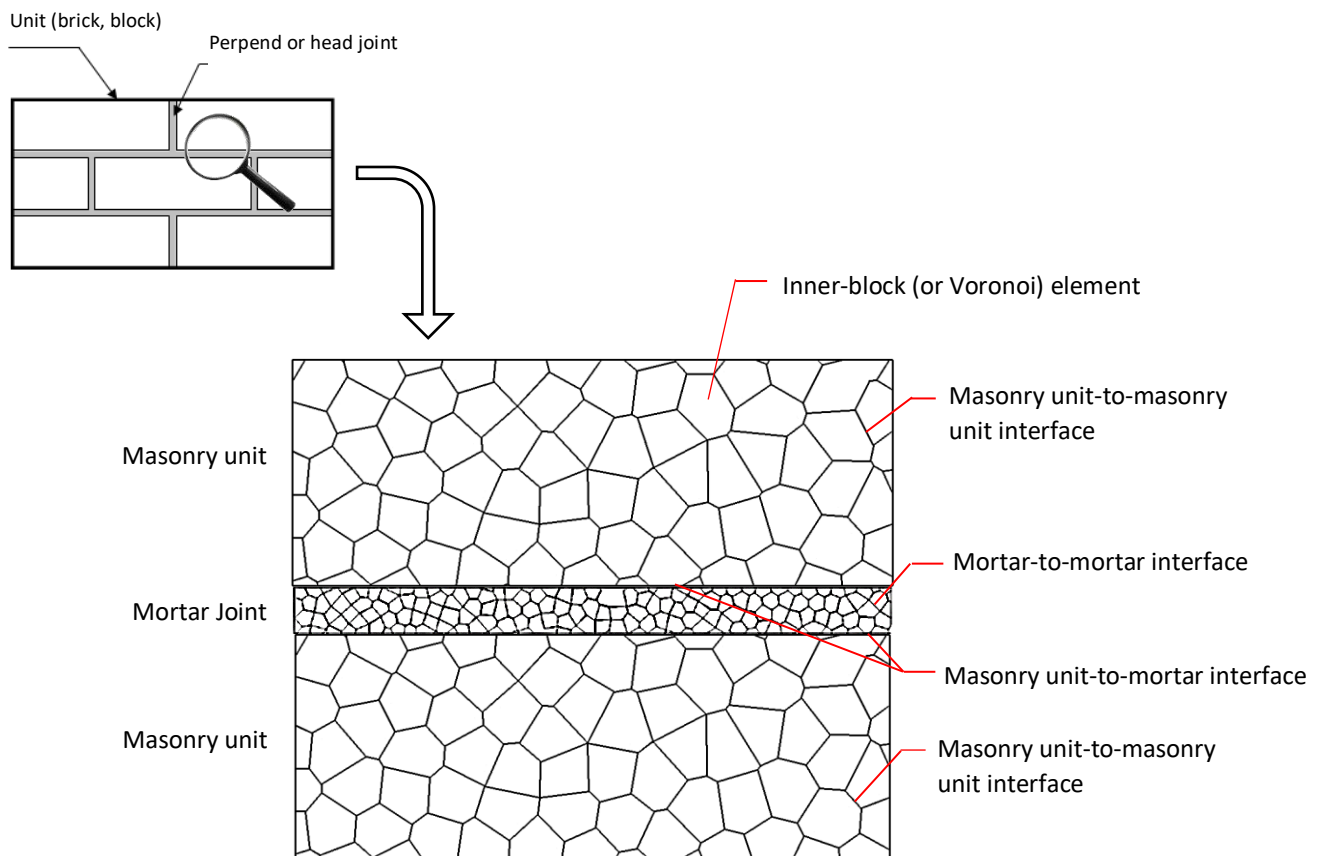

Figure 2. Representation of masonry units and mortar joints by means of polygonal elements
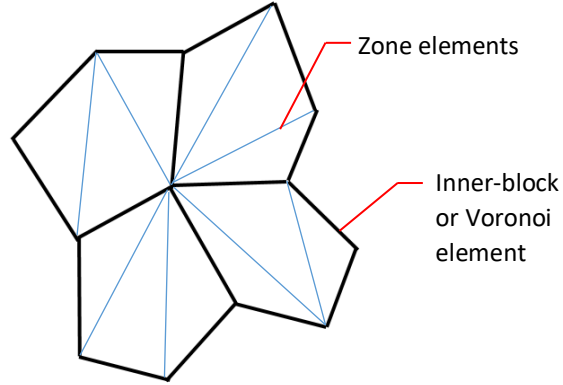
Figure 3. Triangular zones in inner-block elements

2.2 Mechanical representation of joints between inner-blocks

Inner-blocks are bonded together by zero thickness interfaces. Interfaces can be viewed as the location where mechanical interaction between inner-block elements takes place and could be potential fracture slip lines. In the proposed approach, threre are three diffent types of interfaces. These are: a) masonry unit to masonry unit; b) mortar to mortar; and c) masonry unit to mortar (Figure 2). At the interfaces the blocks are connected kinematically to each other by sets of point contacts (Figure 4a), along the outside perimeter of the blocks, at locations where corners or edges meet (Lemos 2007). The main advantages of the point contact hypothesis method are its generality and its simplicity at being able to handle the various types of geometric interaction between the blocks, namely vertex-to-edge contacts, besides the common edge-to-edge interactions along the joints. It can also take into account large block movements, including cases of detachment and re-closure under cyclic loading. For each contact point, there are two spring connections (Figure 4a). These can transfer either a normal force or a shear force from one block to the other (Figure 4b&c). There is no integration of stresses on the contact surface as in FE joint elements (Sarhosis 2012). However, each contact point is assigned an area, and all the areas add up to the total contact surface. Therefore, joint stresses can be evaluated at each point contact, and the standard joint constitutive models, relating normal and shear stresses with joints displacements, can be employed.

In the present paper, a simple constitutive model was assumed for all the contacts, based on a Mohr-Coulomb failure criterion. At each step, trial elastic contact force increments, in the normal and shear direction, are given by Eq. (1) and (2):

$$\Delta F^n = -JKn \times \Delta Un \times A_c \tag{1}$$

$$\Delta F^s = -JKs \times \Delta Us \times A_c \tag{2}$$

where $\Delta F^n, \Delta F^s$ are the normal and the shear force increment (resultant for the contact); JKn, JKs the joint normal and the joint shear stiffness; $\Delta Un, \Delta Us$ the normal and the shear contact displacement increments belonging, defined as the relative displacements between the two blocks at the contact point; and A_c the contact area. The contact area (A_c) allows the conversion between contacts forces and stresses.

The Mohr-Coulomb model employed assumes limited tensile and shear strength, with a brittle failure with a drop from peak to residual strength as soon as either normal or shear failure takes place as illustrated in Figure 4. The chosen model has a limiting tensile strength, Jten. If the tensile strength exceeds the normal stress ($\sigma_n \leq$ Jten), then the normal stress is set to zero ($\sigma_n = 0$) and the interface opens. Alternatively, block elements may overlap at those contacts undergoing compression (Figure 4b). The amount of overlap is controlled by the normal stiffness. Similarly, in shear, the response is controlled by contact shear stiffness (Figure 4c). In addition, in the shear direction, the model uses the explicit incorporation of Coulomb's frictional behaviour (Lourenco 2002). Thus, slippage between bricks will occur when the tangential or shear force at a contact exceeds a critical value τ_{max} defined by:

$$|\tau_s| \leq \text{Jcoh} + \sigma_n \tan(\text{Jfric}) = \tau_{max} \tag{3}$$

, where Jfric is the friction angle and Jcoh the cohesive strength. The Mohr-Coulomb criterion used in this study is the conventional model used to represent shear failure in soils and rocks. Such criterion has been widely used by researchers (e.g. Lourenco 2002) to model the mechanical behaviour of masonry.

After a contact breaks, forces are redistributed and it might cause adjacent contacts to break. During the process, fracture toughness does not control behaviour. Instead, the micro-properties at the inner-block interfaces control the mechanical response of the material and should be calibrated to represent the macro-behaviour. Cracks are initiated at the contact between interfaces. When the stress applied on the contact exceeds either the tensile or shear strength, inner blocks can separate or slide each other. In this way, cracking at the brick, mortar and/or brick-to-mortar interface can be represented.
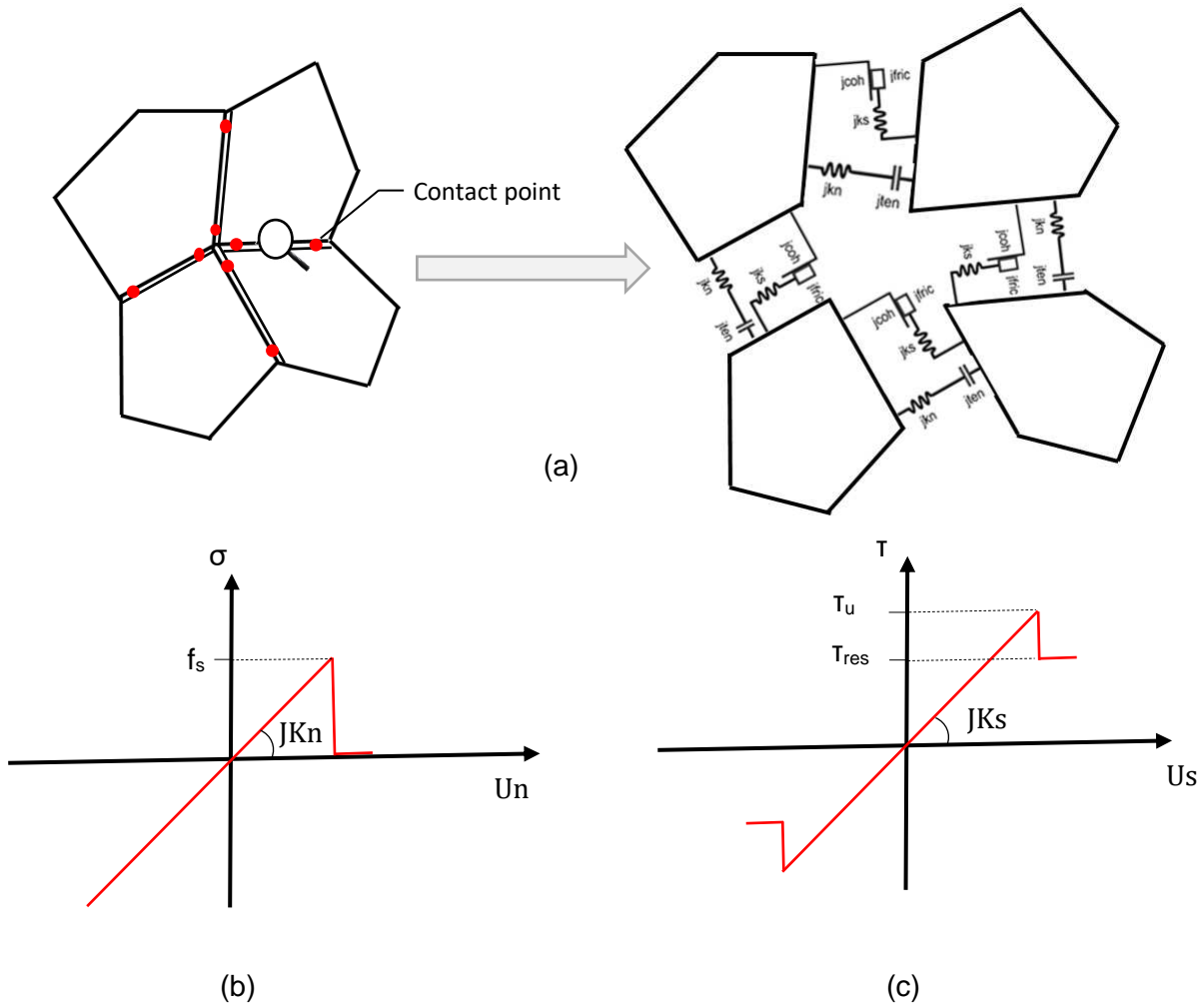
(a)

(b)   (c)

Figure 4. Mechanical representation of the interfaces in masonry units and joints and constitutive law

2.3 Calculation procedure and equations of motion

Following the typical discrete element approach, a dynamic relaxation procedure is used to obtain static solutions. The calculations are made using the force-displacement law at all contacts and the Newton's second law of motion at all blocks nodes. The force-displacement law is used to find contact forces from known displacements, while the Newton's second law governs the motion of the blocks resulting from the known forces acting on the nodes.

Assuming a one-dimensional motion of a single block nodal point acted upon a varying force $F(t)$, Newton's second law of motion can be written in the form:

$$\frac{d\dot{u}}{dt} = \frac{F(t)}{m} \tag{4}$$

where $\dot{u}$ is the velocity; t is the time, and m is the mass. The term F(t) includes all the forces applied to the node, including gravity and external loads, as well as the internal forces from the elements

connected to the node, and the forces from contacts involving the node or its adjacent edges. At time t the central difference scheme can be written as:

$$\frac{d\dot{u}}{dt} = \frac{\dot{u}^{(t+\frac{\Delta t}{2})} - \dot{u}^{(t-\frac{\Delta t}{2})}}{\Delta t} \tag{5}$$

Substituting equation (4) to (5) and rearranging, it gives:

$$\dot{u}^{(t+\frac{\Delta t}{2})} = \dot{u}^{(t-\frac{\Delta t}{2})} + \frac{F(t)}{m}\Delta t \tag{6}$$

In addition, at the end of the time-step, the displacements can be expressed as:

$$u^{(t+\Delta t)} = u^t + \dot{u}^{(t-\frac{\Delta t}{2})}\Delta t \tag{7}$$

Since contact distributed force and relative displacement in the contact are related, the force-displacement calculation is carried out simultaneously (i.e. at the same computational time). In the two dimensional space in which blocky particles are subjected to several forces from external forces, neighbouring particles and gravity, the velocity equations become:

$$\dot{u}_i{}^{(t+\frac{\Delta t}{2})} = \dot{u}_i{}^{(t-\frac{\Delta t}{2})} + \left(\frac{\Sigma F_i^{(t)}}{m} + g_i\right)\Delta t \tag{8}$$

The new block node location is calculated using the known velocities at equations (8).

$$x_i{}^{(t+\Delta t)} = x_i{}^{(t)} + \dot{u}_i{}^{(t+\frac{\Delta t}{2})}\Delta t \tag{9}$$

Where x_i are the node coordinates, respectively. In each time-step, new positions of particles produced which generate new contact forces. Accelerations are also calculated based on the resultant forces and moments at each time step. The procedure is repeated until a satisfactory state of equilibrium achieved e.g. when the net nodal force vector at each centroid of rigid bocks or grid-point of deformable blocks is almost zero (i.e. 0.01% of the initial force) (UDEC 2004).

Convergence to static solutions is obtained by means of adaptive damping in which viscous damping forces acting on the nodes of the deformable blocks or on the rigid block centroids are used, but the viscosity constant is continuously adjusted in such a way that the power dissipated by damping is a given proportion of the rate of change of kinetic energy in the system. The central difference method is only conditionally stable. To avoid numerical instabilities, a limiting time step is defined and the user is allowed only to decrease it. In case of deformable blocks, the limiting time step is calculated, by analogy to a simple degree-of-freedom linear elastic system, for each block node as:

$$\Delta t_n = frac\ 2 \cdot \left(\frac{M_n}{K_n}\right)^{0.5} \tag{10}$$

where M_n is the nodal mass, and K_n is the sum of the stiffnesses of all the elements and contacts connected to the node, and $frac$ is a user-defined factor that maybe used to reduce the time-step (UDEC 2004). The time step for the analysis is the minimum value for all the nodes.

3. Development of the computational models to simulate small scale experimental tests on masonry couplets and prisms

To demonstrate the effectiveness of the proposed approach, results from experimental tests on masonry couplets and prisms are used and compared against those obtained from the numerical model developed. Extensive information of the development of the computational models and comparisons with experimental results are presented below.

3.1 Direct tensile strength

Tensile stresses can occur in masonry due to in-plane loading effects caused by eccentric gravity loads, thermal or moisture movements, foundation movement etc. Figure 5a shows a typical stress-strain diagram of a deformation controlled direct tension test. From this Figure 5a, the behaviour prior to attaining the peak load is a close approximation to linear elastic behaviour while tension-softening behaviour after tensile failure is observed. Tensile failure can occur either at: a) brick-mortar interface (Figure 5b); or b) mortar; and/or both brick-mortar interface and mortar (Figure 5c).
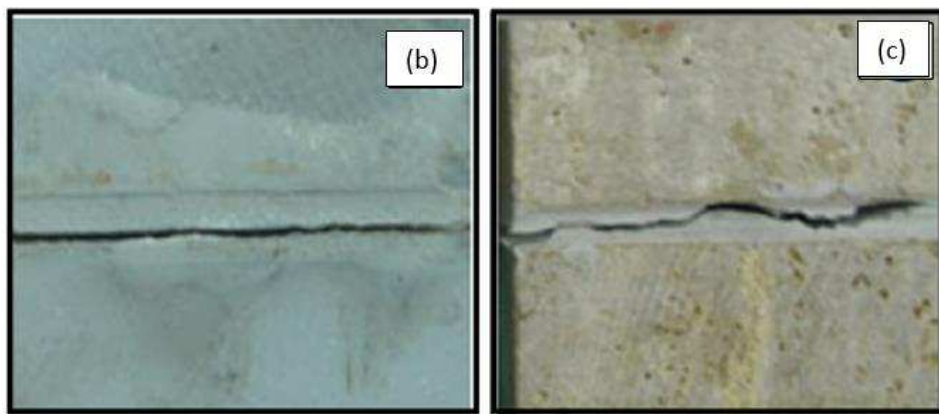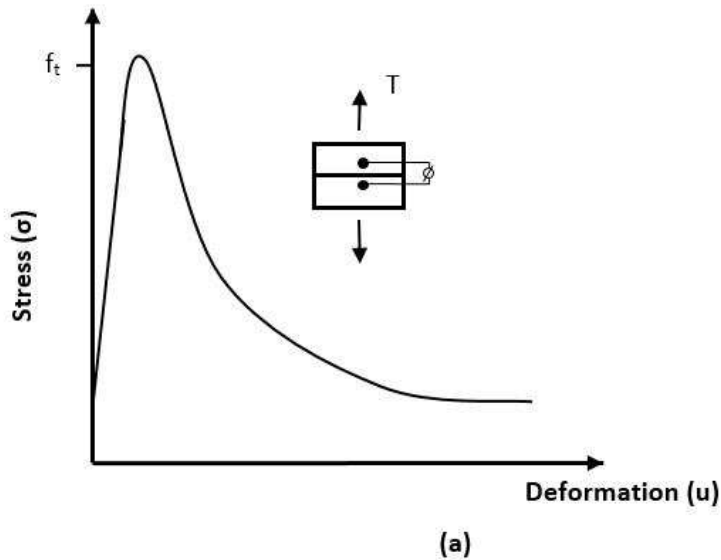

Figure 5. Schematic diagram of a deformation controlled direct tension test (a); Failure modes derived from direct tensile strength test: (b) tensile failure of the bottom brick to mortar interface; (c) cracking of mortar (after Adami and Vintzileou, 2008)

The ability of the proposed computational modelling approach to capture the stress against displacement and failure mode of a deformation controlled direct tensile strength test was evaluated by comparing the numerical against the experimental test results obtained by Van der Pluijm (1992). In the experiment, clay bricks were wire-cut (wc-jo) with dimensions 100 mm × 50 mm × 50 mm (length × breadth × width). The mortar joint was 15 mm thick and composed of 1:1:6 (OPC:Lime:Sand). The experimental set up and the tensile strength against displacement of four tests carried out in the laboratory are shown in Figure 6. Experimental results show the displacements measured with the LVDTs placed at the corners of the specimen.
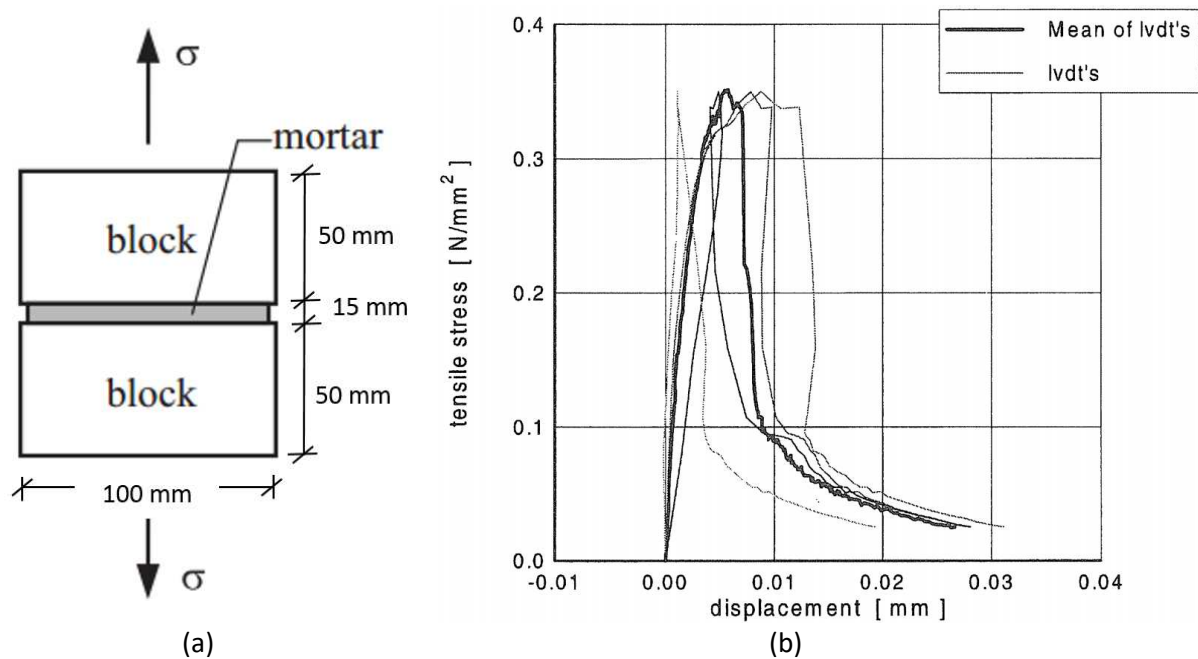

Figure 6. Experimental test specimen (a) and tensile stress against displacement relationship of the unit-mortar interface in direct tension (b); Tensile stress (f_t) is 0.35 N/mm^2 (Van der Pluijm, 1992).

Geometric models representing the specimen tested in the laboratory were created in the computational model (Figure 7a). Bricks were represented by deformable blocks, assumed elastic, and divided into a regular mesh of triangular zones. The mortar joint were represented by an assemblage of Voronoi elements, approximately 2 mm in size. The Voronoi elements are also discretized into triangular zone elements (Figure 7b), each assumed to behave in a linear elastic manner and characterized by Young's modulus, Poisson ratio and bulk density. Material properties of the brick and mortar were obtained from Van der Pluijm (1992) and shown in Table 1. The calibrated material properties used for the development of the computational model are shown in Tables 2 & 3. These represent the micro-properties of the mortar and brick-to-mortar interface. At first, the model was brought into a state of equilibrium under gravity. Then, an external load was applied by assigning a controlled upward vertical velocity at the top masonry unit which was equal to 0.02 mm/s. Simulations were undertaken and indicated that for values below 0.02 mm/s, the loading rate had negligible effects on the simulated peak tensile strength. Tensile strength was calculated by dividing the maximum upward force by the cross sectional area of the masonry unit.

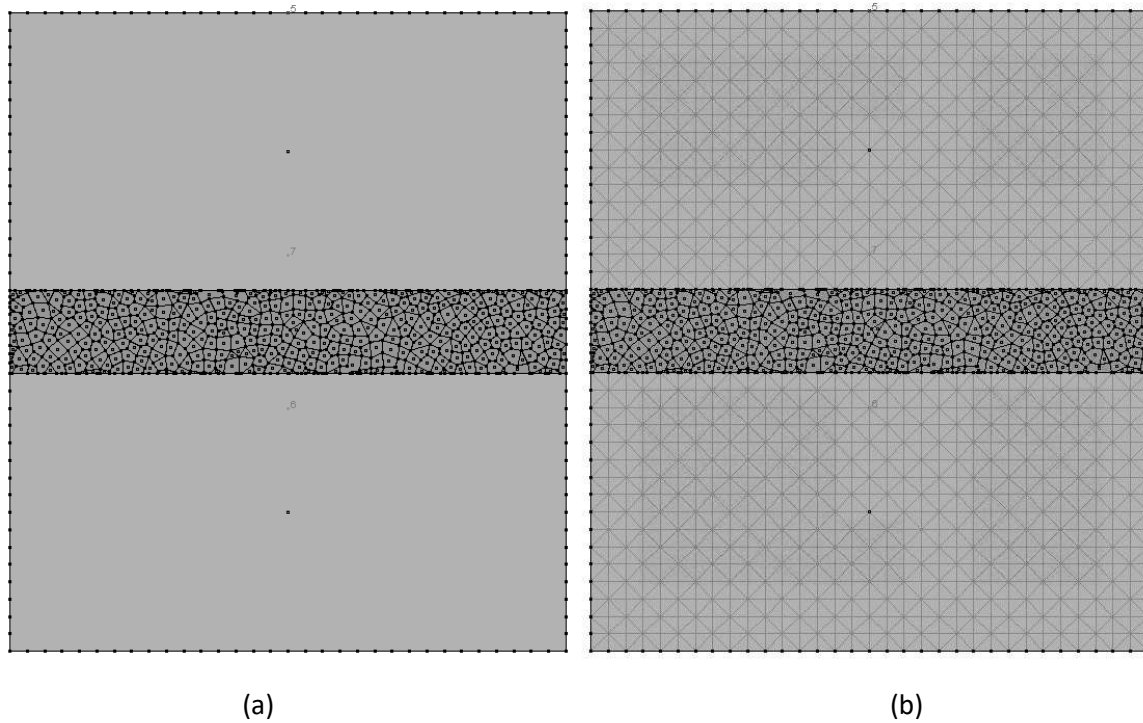Also, the average relative displacement across the mortar joint was recorded throughout the simulations.

(a)   (b)

Figure 7. Construction of the computational model: (a) Geometry of the tensile test; and (b) finite-elements in the brick and mortar

Table 1. Macro-properties of the brick and mortar block elements (Van der Pluijm, 1992)

Brick properties			Mortar properties		
Young's Modulus (N/m^2)	Poisson's ratio	Density (kg/m^3)	Young's Modulus (N/m^2)	Poisson's ratio	Density (Kg/m^3)
16,700 x 10^6	0.2	1,900	2,974 x 10^6	0.2	1,250

Table 2. Mortar-to-mortar (M-M) joint interface micro-properties

Joint Normal Stiffness (JKn) N/m^3	Joint Shear Stiffness (JKs) N/m^3	Joint frictional resistance (Jfic) deg	Joint cohesive strength (Jcoh) N/m^2	Joint tensile strength (Jten) N/m^2	Joint dilation (Jdil) deg
400 x 10^9	200 x 10^9	38	0.75 x 10^6	0.75 x 10^6	4

Table 3. Brick-to-Mortar (B-M) joint interface properties

Joint Normal Stiffness (JKn) N/m^3	Joint Shear Stiffness (JKs) N/m^3	Joint frictional resistance (Jfic) deg	Joint cohesive strength (Jcoh) N/m^2	Joint tensile strength (Jten) N/m^2	Joint dilation (Jdil) deg
400 x 10^9	200 x 10^9	38	0.60 x 10^6	0.60 x 10^6	4

Figure 8 compares the experimental against the numerical results. Two numerical simulations were carried out. In the TT1 simulation, different micro-mechanical properties were assumed for the brick-mortar (B-M) interface and mortar-to-mortar (M-M) interface (Tables 2 and 3). In the TT2 simulation, the micro-properties of the brick to mortar (B-M) interface were the same as those of the mortar-to-mortar (M-M) interface (Table 3). From Figure 8, the numerical model is capable to obtain the peak tensile stress obtained from the experimental study. Also, from Figure 8, the peak tensile strength obtained from the TT1 simulation is lower than those obtained from the TT2. This is because the selected micro-mechanical properties of the cohesive and tensile strength of the brick to mortar interface (0.6 N/mm^2) were smaller to those at the mortar-to-mortar interface (0.75 N/mm^2). In addition, in TT1 simulation, failure occurred at the brick-to-mortar interface while for the TT2 simulation failure occurred at both mortar and brick to mortar interface (Figure 9). The evolution of cracking for the two different cases studied is shown in Figure 16a, b, c for the TT1 case. Cracking initiated at the bottom right hand side brick to mortar interface and propagated to the right hand side. Figure 16 d, e, f present the evolution of crack pattern for the TT2 case where cracking initiated from the bottom right hand side of the brick to mortar interface and propagated in the mortar itself to the right hand side.
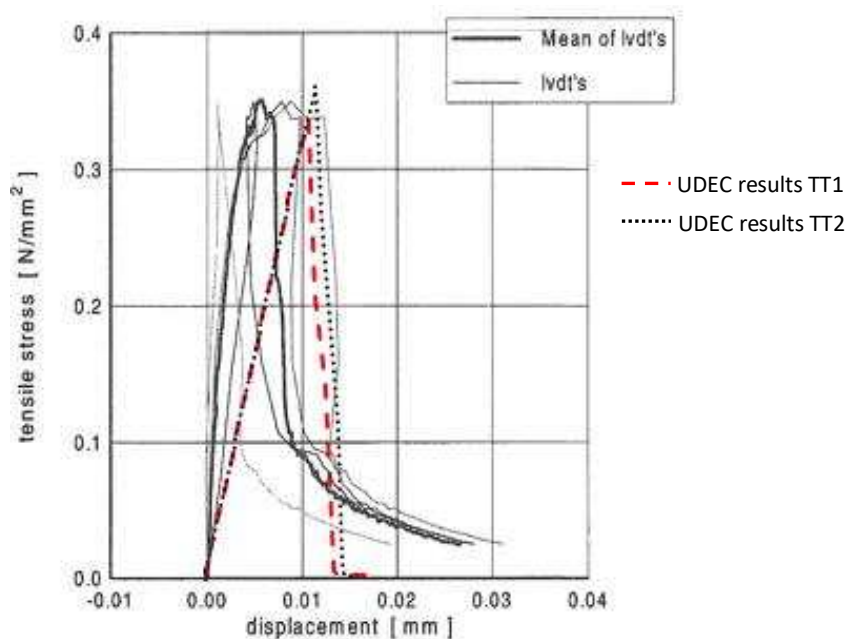

Figure 8. Comparison of numerical against experimental results of the tensile test from the wc-jo, 1:1:6 series.
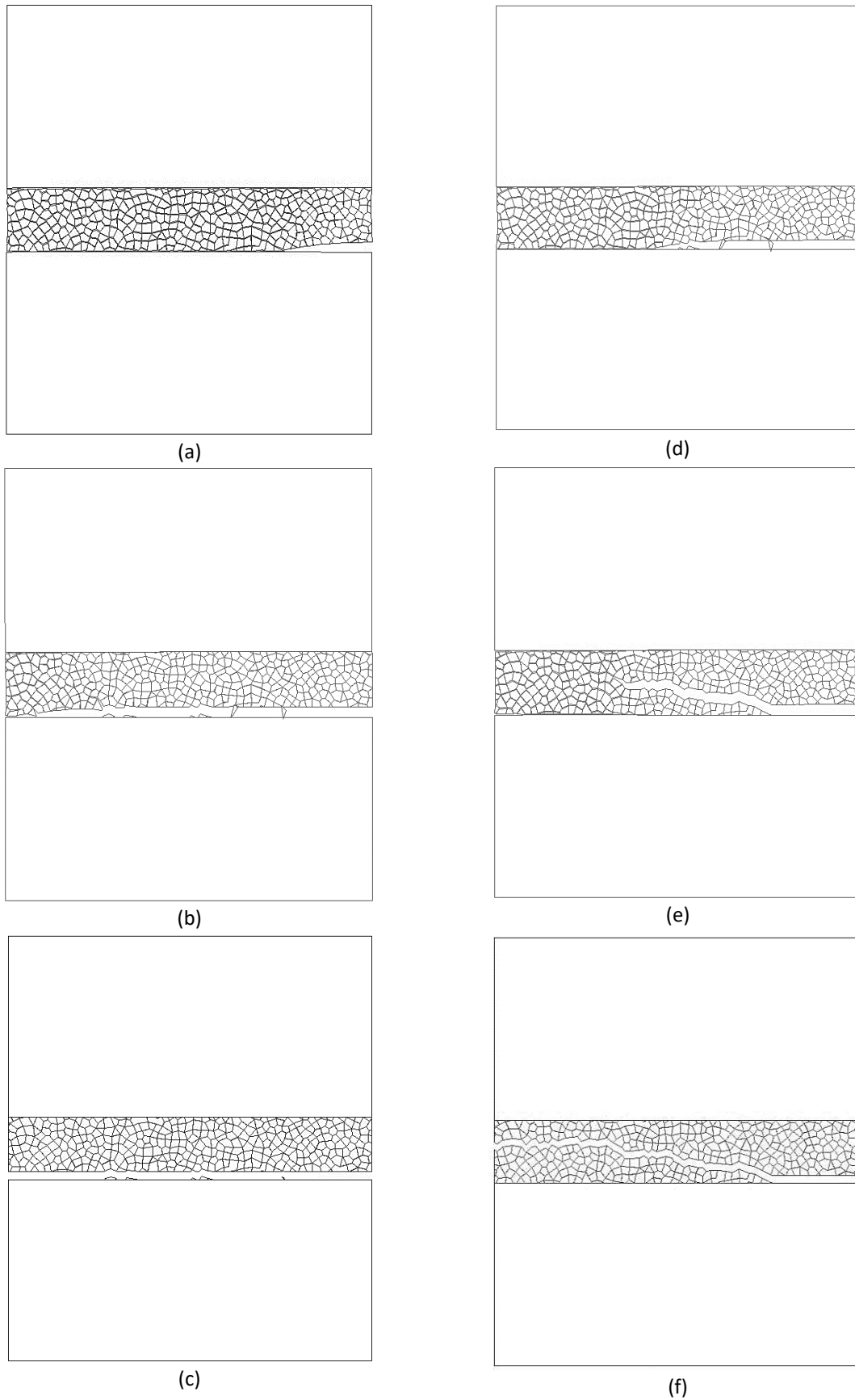
Figure 9. Crack propagation as observed from the TT1 and TT2 numerical simulations: (a, b, c) is for the TT1 (Failure at the B-M interface); and (d, e, f) for the TT2 (Failure at the mortar and B-M interface)

In addition, the influence of the size of the Voronoi elements on the peak tensile strength and failure mode were investigated. Figure 10 compares the numerical against experimental tensile strength results when the size of the Voronoi elements is 2 mm (TT2 simulation) and 6 mm (TT3 simulation). In all cases, material properties have been kept the same as those shown in Table 1, 2 and 3. From Figure 10, the numerical model constructed with larger Voronoi elements has a stiffer elastic slope. This is due to the fact that for both models, the same inner-element Young's modulus and joint stiffness were used. To improve the approximation, the elastic slope can be easily calibrated for a given Voronoi size by changing the joint stiffness parameters. From Figure 10, when the size of the Voronoi elements is 6mm, the peak tensile strength is 0.43 N/mm^2, which is higher when compared for the case where the Voronoi element is 2 mm and the peak strength is 0.35 N/mm^2. Again, the desired macroscopic strength can be obtained by properly calibrating the joint strength micro-parameters. Furthermore, Figure 11 compares the failure mode for the different in size Voronoi elements. From Figure 11, it appears that for these two cases, the failure mode has a phenomenologically similar pattern of development. For both cases, initially cracking appeared at the bottom brick to mortar interface. With the application of further external load, the crack propagated in the mortar itself.
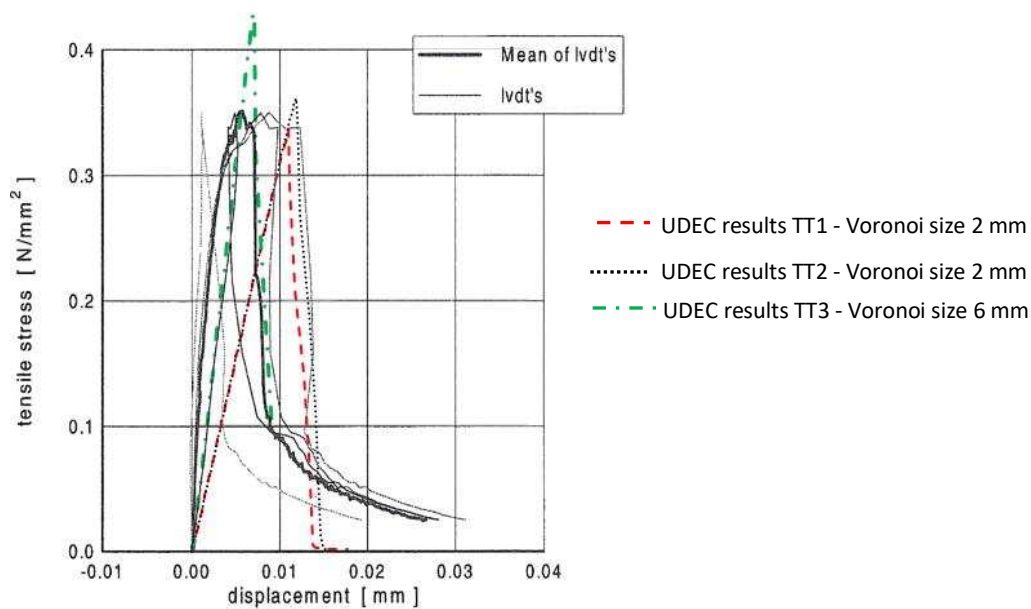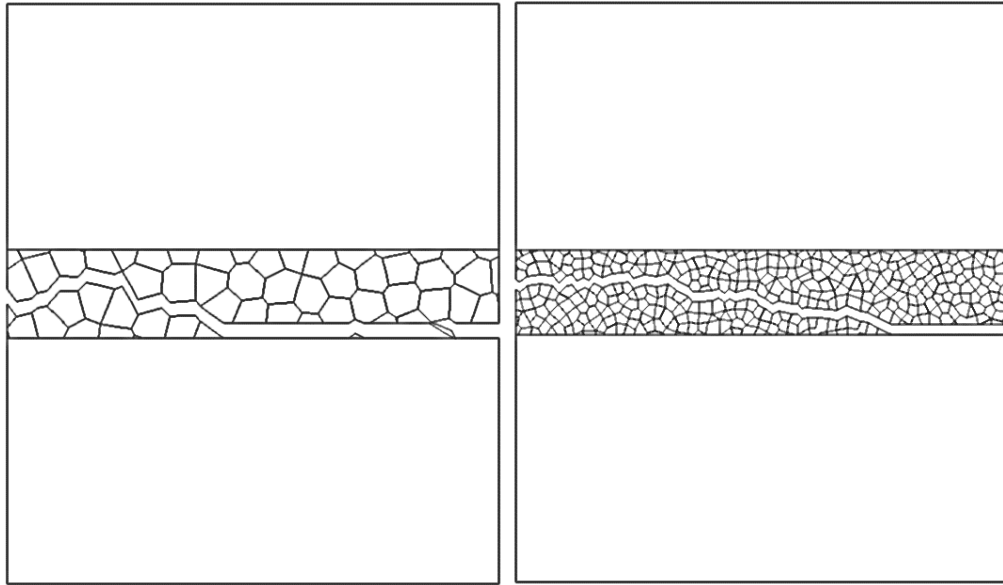

Figure 10. Influence of Voronoi size on the tensile strength.

(a) Voronoi element size is 6 mm (TT3)   (b) Voronoi element size is 2 mm (TT2)

Figure 11. Failure mode as obtained from the numerical model for different in size Voronoi elements

3.2 Shear behaviour of bed joints

The strength of masonry in combined shear and compression is of importance in relation to understanding the resistance of masonry to lateral loading. Several tests on masonry panels and specimens subjected to this type of loading have been carried out (Figure 12). A discussion regarding the adequacy of the different test methods will not be given here; the reader is referred to Atkinson et al. (1989) and Jukes and Riddington (1997) for further information about the types of shear strength tests.
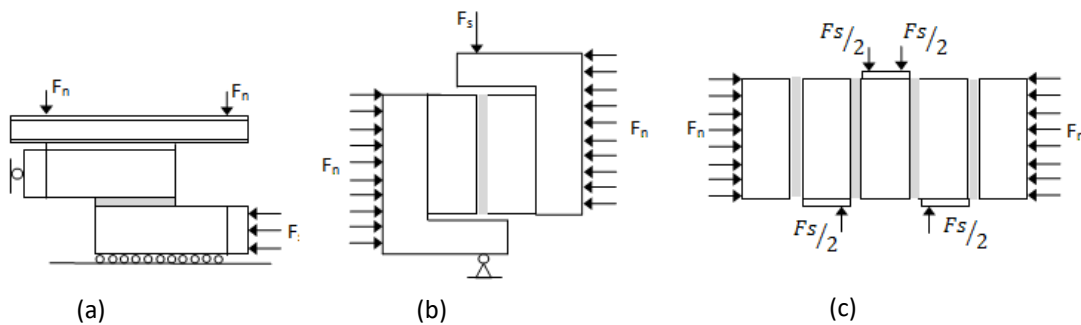

(a)   (b)   (c)

Figure 12. Different types of shear tests for masonry: a) direct shear test; b) Van der Pluijim test (Van der Pluijim, 1999); and c) triplet test

For a shear test with normal pre-compression, the relationship between the shear stress and the shear displacement is of the form shown in Figure 13a. Such behaviour shows a great similarity with the behaviour under tension (Figure 5a), except that there is a residual shear strength (τ_{fr}) after failure; which is not the case with a tensile failure. The amount of τ_{fr} will depend on the applied compression. The descending part of the graph between ultimate shear strength (τ_u) and the frictional resistance (τ_{fr}) is described by Van der Pluijm (1999) as softening of the cohesion. Also, in

Figure 13a, normal stress is denoted as (σ), shear stress (τ) and the horizontal displacement as (u). Experimental evidence has shown that depending on the strength of the mortar and brick to mortar interface, failure can occur either at the brick to mortar interface (Figure 13b) and/or both brick to mortar interface followed by a diagonal shear crack at mortar (Figure 13c).
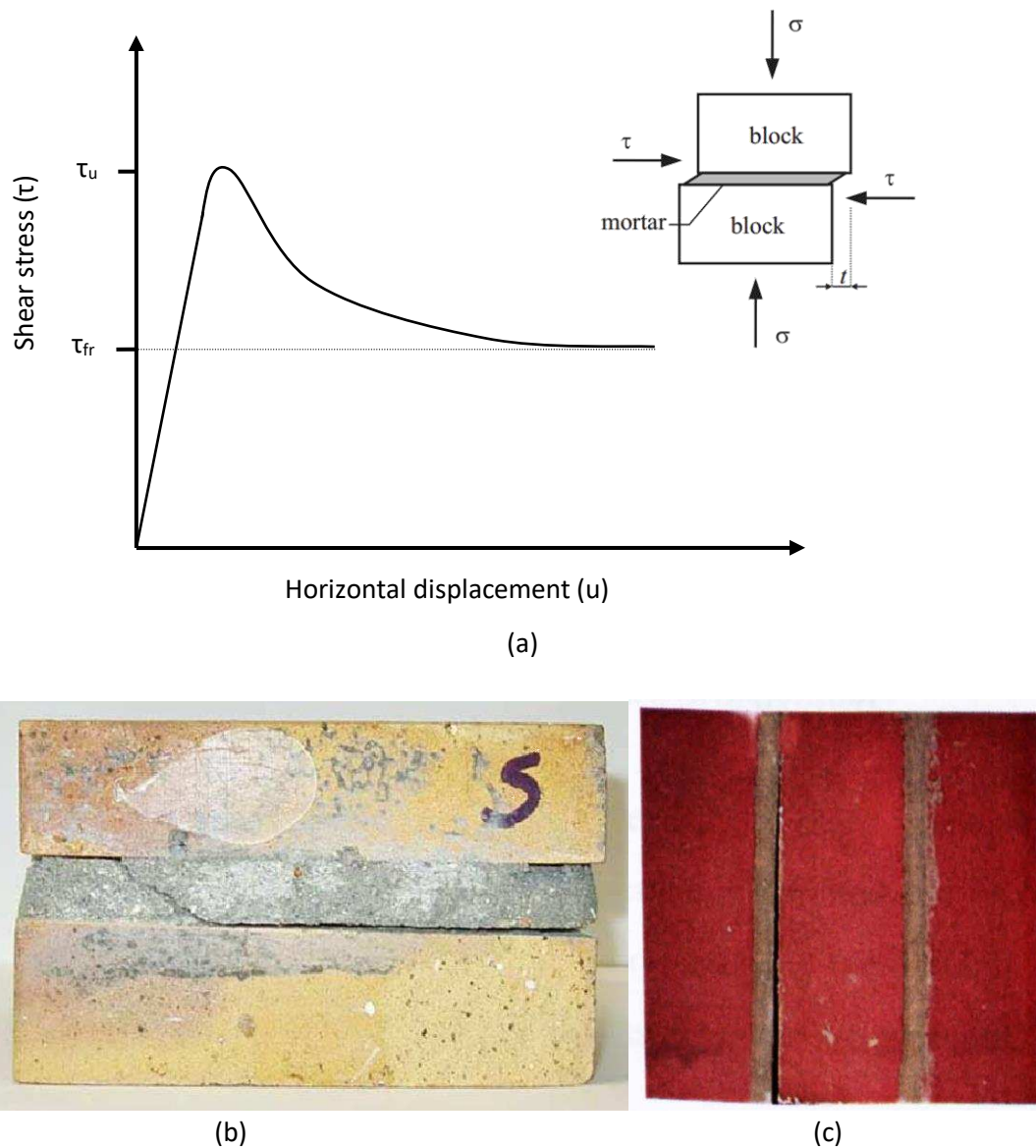

(a)

(b)

(c)

Figure 13. Characteristics of shear strength tests: (a) Schematic shear stress against shear displacement relationship of a deformation controlled shear test under constant normal compression (Van der Pluijm, 1993); (b) Diagonal shear failure of the mortar joint during direct shear test (Abdou et al., 2006); (c) Failure at the brick to mortar interface during a triplet shear test (Beattie, 2003)

The ability of the discrete element model to capture the main features related to the shear behaviour of mortar joints under horizontal shearing and vertical pre-compression was evaluated by comparing the numerical against the experimental results of a deformation-controlled experimental test carried out by Van der Pluijm (1993). In the experiment, clay bricks were wire cut (Wc-J090; as

annotated by Van der Pluijm (1993) with dimensions 200 mm × 50 mm × 50 mm (length × breadth × width). The mortar joint was 15 mm thick and composed of 1:2:9 (OPC:Lime:Sand); where OPC is Ordinary Portland Cement. In the experiment, the friction angle of the mortar was 1.01, the ultimate shear strength (τ_u) was 0.87 N/mm^2 and the residual frictional strength (τ_{fr}) was 0.73.

Geometric models representing the experimental set up were created in the computational model (Figure 14a). Similar to the tensile strength test, bricks were model by deformable blocks bonded together by mortar represented by an assemblage of 3.5 mm in size Voronoi elements. Both blocks and Voronoi elements discretized into zones (Figure 14b), each assumed to behave in a linear elastic manner. The properties of the brick and mortar block elements are shown in Table 4. In addition, the calibrated micro-properties of the mortar-to-mortar interface properties are shown in Table 5. First, the model was brought into equilibrium under gravitational load. Then, an external velocity equal to 0.2 mm/s was applied at the upper brick while the bottom brick was fixed in the horizontal and vertical direction. In addition, three different pre-compressions with magnitude 0.1, 0.5 and 1 N/mm^2 applied at the top of the upper brick separately. Figure 15 compares the numerical against the experimental shear stress versus shear displacement relationships. From Figure 15, the numerical model is capable to predict the peak and residual shear strength with reasonable accuracy. In addition, the failure mode as obtained from the numerical model for the shear tests using different amount of pre-compression is shown in Figure 16.
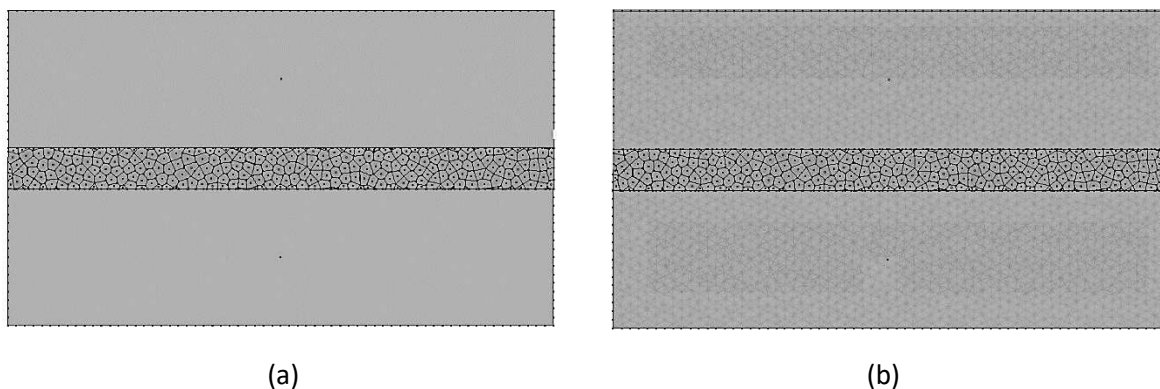

| (a) | (b) |

Figure 14. Construction of the computational model: (a) Geometry of the direct shear strength test; (b) finite-elements in the brick and mortar

Table 4. Macro-properties of the brick and mortar block elements (Van der Pluijm, 1992)

Brick properties			Mortar properties		
Young's Modulus (N/m^2)	Poisson's ratio	Density (kg/m^3)	Young's Modulus (N/m^2)	Poisson's ratio	Density (kg/m^3)
16,700 x 10^6	0.2	1,900	2,974 x 10^6	0.2	3,250

Table 5. Joint interface micro-properties (M-M properties are same as B-M properties)

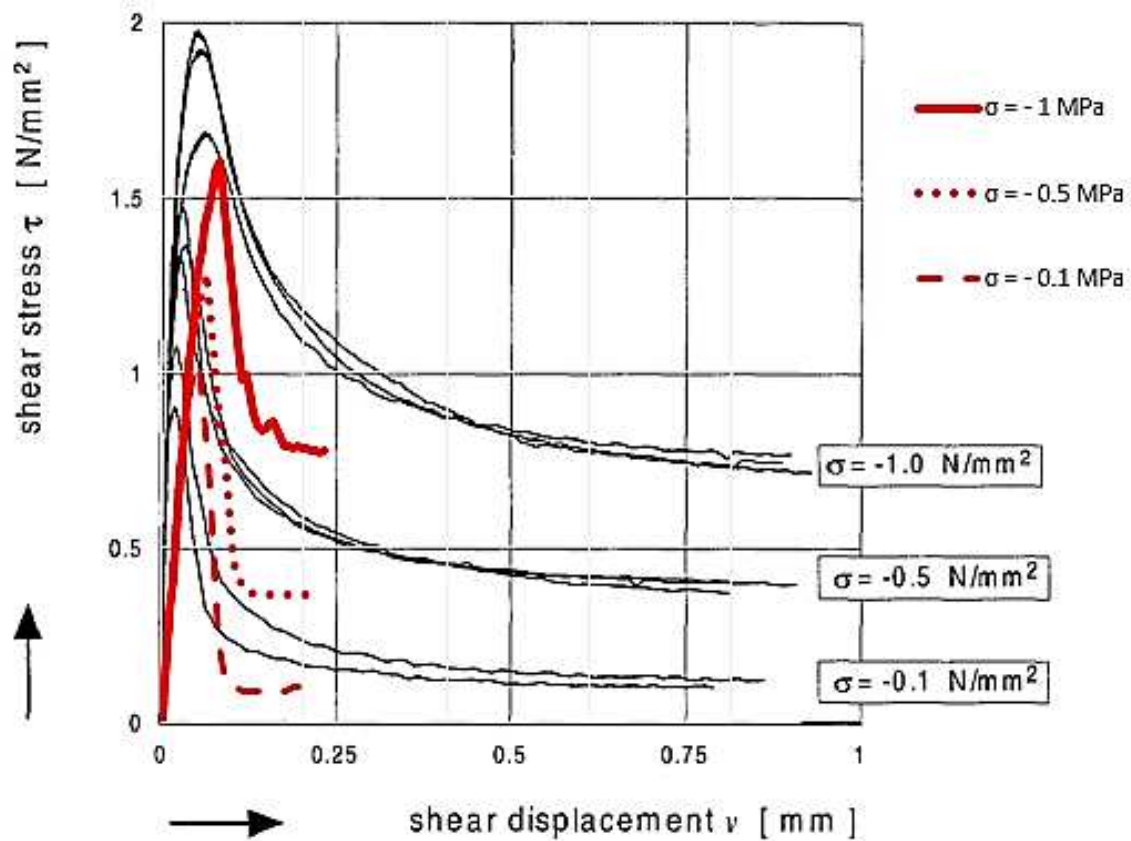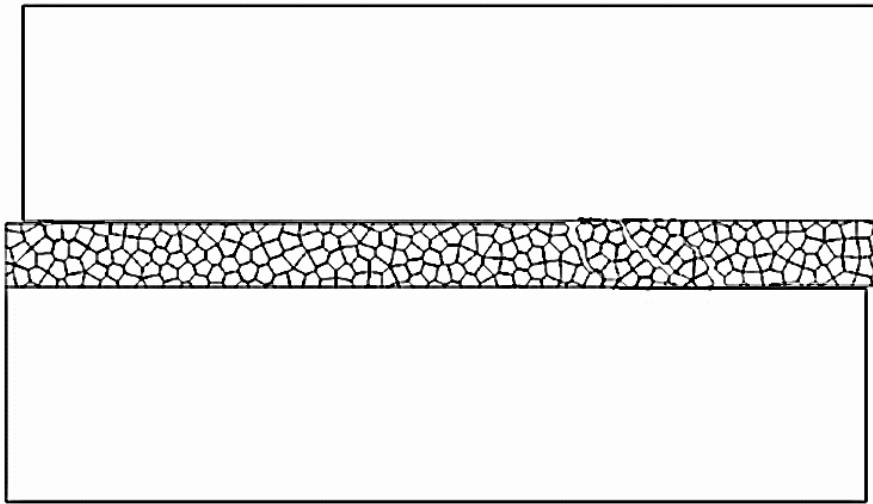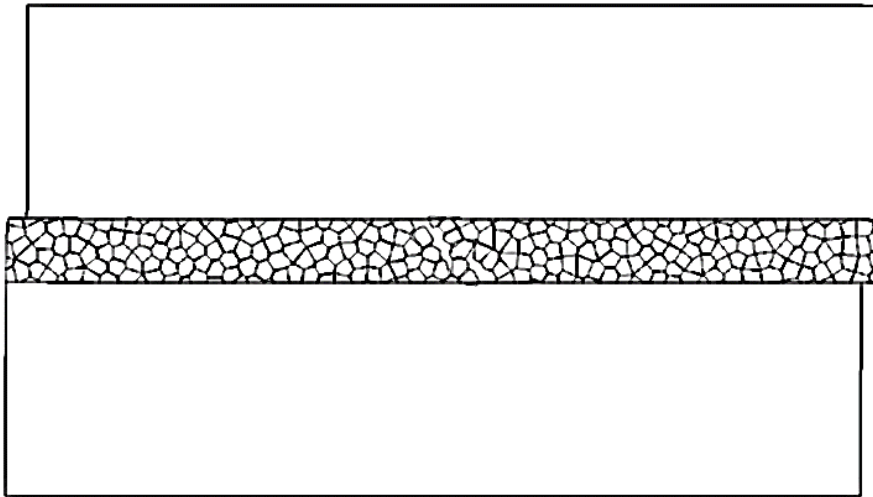| Joint Normal Stiffness (JKn) N/m³	Joint Shear Stiffness (JKs) N/m³	Joint frictional resistance (Jfic) deg	Joint residual frictional resistance (Jfric_res) deg	Joint cohesive strength (Jcoh) N/m²	Joint tensile strength (Jten) N/m²	Joint dilation (Jdil) deg
400 x 10⁹	200 x 10⁹	45	36	3 x 10⁶	1.5 x 10⁶	0

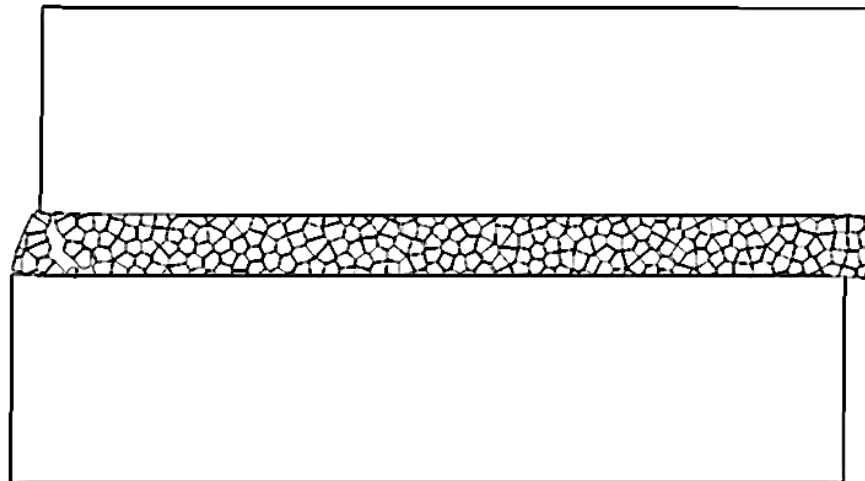**Figure 15.** Comparison of experimental against numerical results for the direct shear test

a) Vertical pre-compression σ = 0.1 N/mm²

b) Vertical pre-compression σ = 0.5 N/mm²

c) Vertical pre-compression σ = 1 N/mm²

Figure 16. Failure mode as obtained from the numerical model for the shear tests using different pre-compression

3.3 Compressive uniaxial behaviour

Since masonry structures are primarily stressed in compression, there has been an extensive concentration of interest to understand their compressive strength. A series of experimental tests have been carried out on standardized masonry prisms subjected to direct compression (Hendry 1998; Oliveira 2003). Although compressive strength tests on masonry prisms do not necessarily reproduce the state of stress in the actual masonry structure, such tests can be used to obtain values in the selection of design stresses as well as assist in investigating the influence of masonry constituents on the compressive strength. In addition, observations obtained from testing masonry prisms subjected to uniform compression demonstrated that the failure mode of masonry prism depends on the relative strength of mortar compared to the unit. In particular, masonry fails by the development of tension cracks parallel to the axis of loading or due to shear failure along certain lines of weakness (Hendry 1998).

A numerical model has been developed to represent the compressive strength test of a masonry prism carried out in the laboratory by Oliveira (2003). The masonry prism composed of five bricks. The bricks had average dimensions of 285 mm ×130 mm × 50 mm. Joints were all made of cement mortar and had the same thickness and equal to 10 mm. The prism was placed between two steel platens whose friction with masonry unit is negligible and subjected to an axial control displacement until failure. The material characteristics of the prisms are shown in Table 6. Figure 17 shows the geometry of the masonry prisms tested in the laboratory.
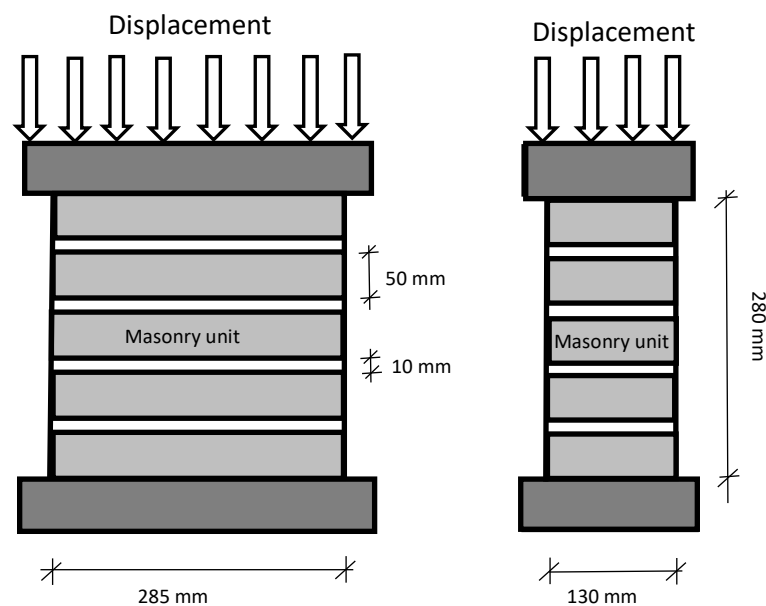

Figure 17. Geometry of the masonry prism tested in the laboratory (Oliveira 2003)

Table 6. Material characteristics of prisms as obtained from the experimental study (Oliveira 2003)

Modulus of elasticity Ex = Ey (N/m^2)	Poisson coefficient v_{xy}	Compression strength (N/m^2)	Fracture Energy (N/m)
4100 x 10^6	0.20	27.5 x 10^6	23,000

Geometric models representing the specimen tested in the laboratory were created in the computational model (Figure 18a). Both bricks and mortar represented by an assemblage of different in size deformable Voronoi elements (Figure 18b). Bricks were assembled with a 10 mm size of Voronoi elements while mortar joints with a 3 mm size Voronoi elements. Figure 31, represents the different interfaces used in the numerical model. Also, the material properties used for the calibration of the computational model are shown in Tables 7, 8 and 9. The analyses here reported were performed in a non-associated plasticity context, assuming a dilatancy equal to zero. Similar values have been reported by Lourenco and Rots (1997) and Henriques & Lourenco (2005). According to their studies, non-zero dilatancy associated with the symmetry boundary conditions adopted in the simulations could induce high normal stresses and locking of the particles, resulting in increasing strength.

The masonry prism has been confined by two steel platens, modelled as rigid blocks. A velocity has been applied on the top of the steel platen and reaction forces were continuously recorded as the sample axial force. The loading rate was set to maintain a displacement of 0.01 mm/s and a high damping applied so that the sample remains in a quasi-static condition. Figure 19 compares the numerical against the experimental test results, showing a good agreement. In addition, Figure 20 shows the failure mode obtained from the experimental study against the one obtained from the numerical simulations. From the numerical simulations it was observed that the peak appears to take place when one of the bricks splits in two by coalescence of the vertical tensile cracks that progressively develop. Total failure followed when the resisting core started to break. In general, the numerical model displays a more brittle response compared with the gradual softening observed in the experiment. The model performance may be improved by elaborating the contact constitutive laws, with the incorporation of softening behaviour calibrated to provide a closer approximation to the experimental fracture energies. In addition, the model could be improved by giving a random scatter to the appropriate material characteristics of the contacts. In addition, during compression, the shear stresses at the brick-mortar interface result in an internal state of stress which consists of trialxial compression in mortar and bilateral tension coupled with axial compression in bricks. This state of stress results in vertical splitting cracks in bricks at the middle of the masonry prism. Therefore, deformation at the middle of the prism is more eminent than at the top of the prism (Figure 20e). Similar findings are also reported by various experimental studies carried out by Atkinson and Noland (1983) and Drysdale et al. (1994).
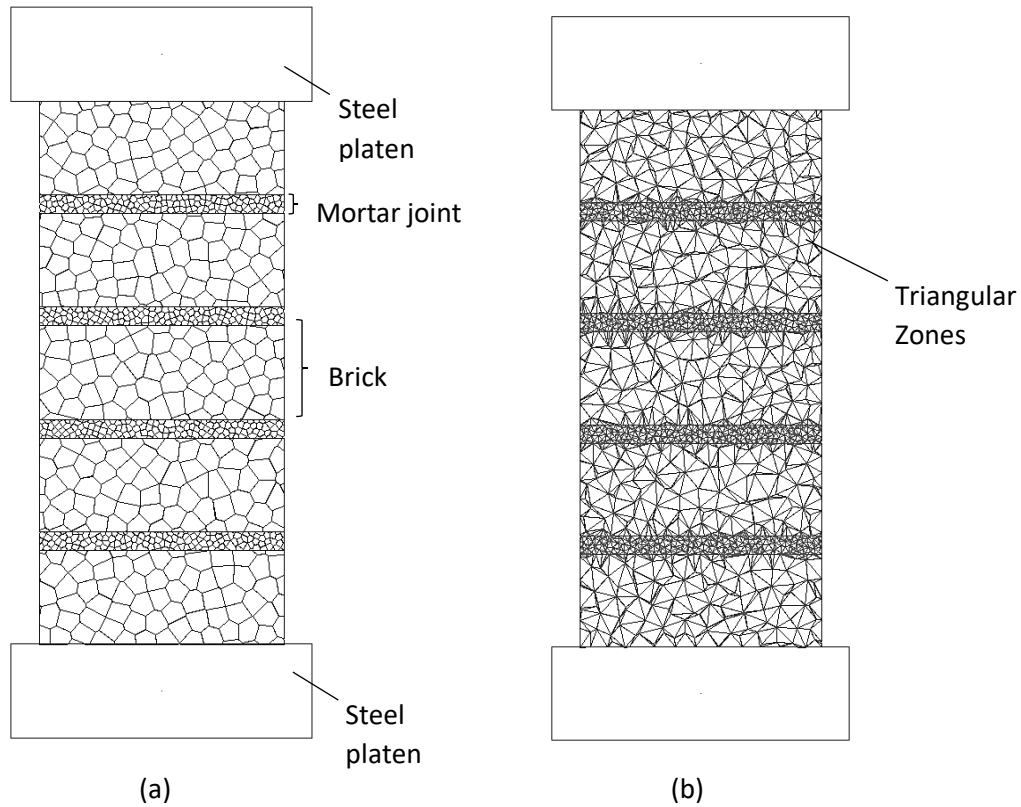
Figure 18. Computational model: (a) Geometry of the prism; (b) Triangular zones in the brick and mortar

Table 7. Macro-properties of the brick and mortar block elements

Brick properties			Mortar properties		
Young's Modulus (N/m^2)	Poisson's ratio	Density (Kg/m^3)	Young's Modulus (N/m^2)	Poisson's ratio	Density (Kg/m^3)
20×10^9	0.2	2,000	5.8×10^9	0.2	2,000

Table 8. Mortar to mortar and brick to mortar interface micro-properties

Joint Normal Stiffness (JKn) N/m^3	Joint Shear Stiffness (JKs) N/m^3	Joint frictional resistance (Jfric) deg	Joint cohesive strength (Jcoh) N/m^2	Joint cohesive residual strength (Jcoh_res) N/m^2	Joint tensile strength (Jten) N/m^2	Joint dilation (Jdil) deg
348×10^9	174×10^9	15	1.4×10^6	0.28×10^6	0.7×10^6	0

Table 9. Brick to brick interface micro-properties

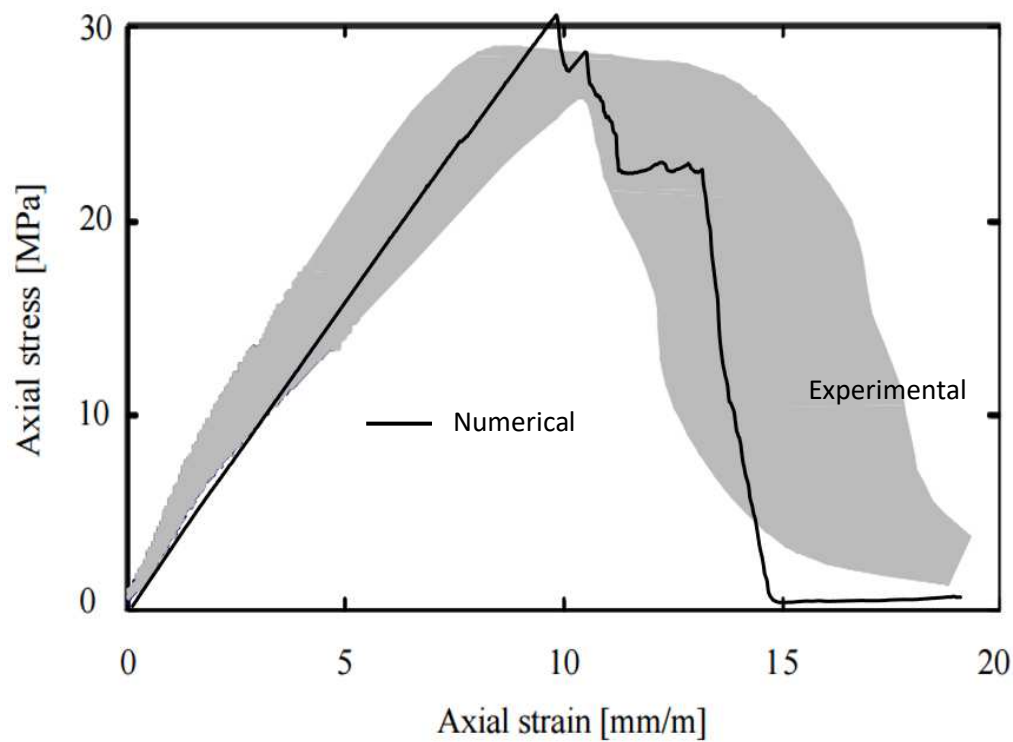| Joint Normal Stiffness (JKn) N/m³	Joint Shear Stiffness (JKs) N/m³	Joint frictional resistance (Jfric) deg	Joint cohesive strength (Jcoh) N/m²	Joint cohesive residual strength (Jcoh_res) N/m²	Joint tensile strength (Jten) N/m²	Joint dilation (Jdil) deg
$1{,}260 \times 10^9$	630×10^9	20	15×10^6	3×10^6	7.5×10^6	0

Figure 19. Comparison of experimental against numerical results of monotonic increasing load in compression
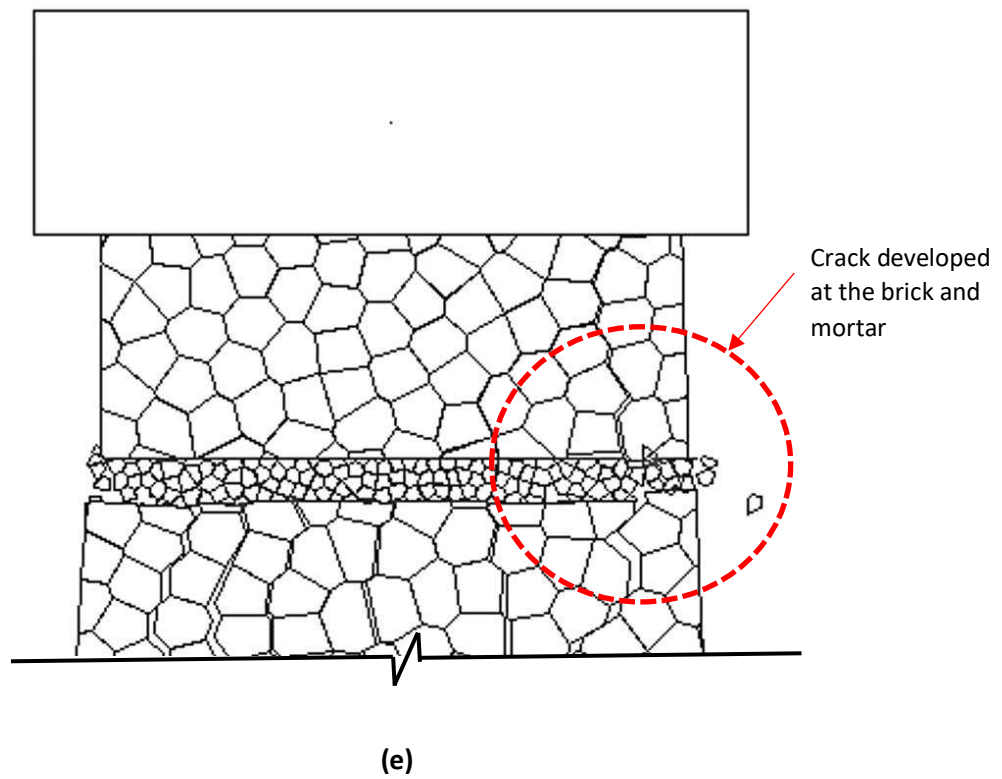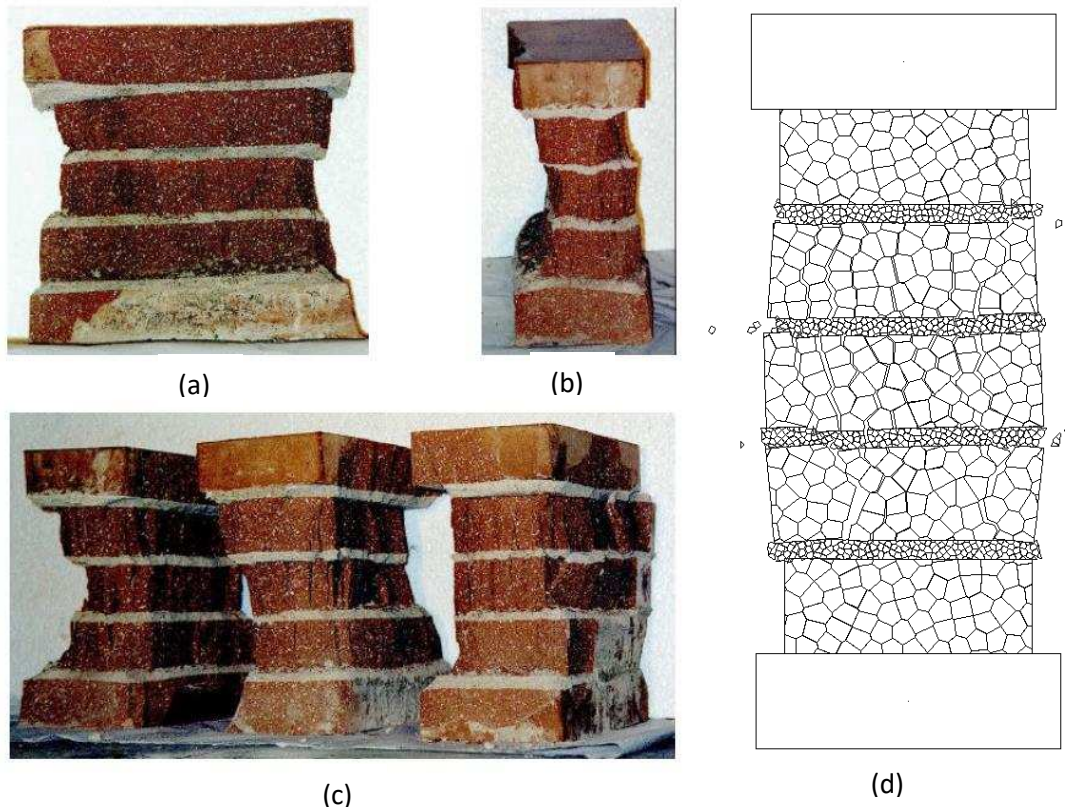
Figure 20. Failure modes of the brick masonry prisms: a) frontal view; b) lateral view; c) perspective of three tested prisms; d) lateral view obtained from the numerical model; e) close up view of the top part of the masonry prism (deformation at the top brick is also evident)

4. Conclusions

Understanding the damage and failure mechanisms of masonry structures can help engineers reduce catastrophic failures and perform effective measures for their repair, strengthening and rehabilitation. This can be achieved by gaining insights on the macro-level strength-deformation behaviour and micro-level defects and crack growth of masonry structures. In this paper, a detailed micro-modelling approach to represent the micro-structure of masonry assemblages has been proposed. The phenomenological discontinuum approach considers masonry units and mortar joints as an assemblage of densely packed discrete irregular particles bonded together by zero thickness interface laws. In this way, the actual dimensions of the masonry units and mortar joints can be considered. The proposed model was discussed in detail and a series of computational models were developed to simulate the mechanical behaviour of small-scale experimental tests commonly used to obtain tensile strength, shear strength and compressive strength of masonry. Stress-strain characteristics and failure modes obtained from the numerical model were compared against the experimental findings. From the results analysis, it is possible to conclude that:

- A fair to good agreement between the experimental and the numerical results was obtained which demonstrates the huge potential of the modelling approach proposed.
- The proposed computational approach shows significant advantages when compared to standard continuum models, since it allows one to observe crack initiation and propagation in a realistic manner. In particular, the approach allows to model cracking as a real discontinuity among particles and not as a modification in the material properties.
- The approach allows failure to occur either at the brick, mortar and/or brick/mortar interface, through a randomly-generated network of potential fractures. Realistic failure mechanisms under tensile, shear and compressive loads were obtained. In this way, further insight into the crack initiation and propagation can be obtained.
- The numerical results were obtained assuming simple contact constitutive laws, which allowed the matching of peak strengths and failure strains. A closer approximation to the stress-strain curves can be attained with more elaborate contact constitutive models.
- Numerical results are dependent on the particle size. Therefore, in the calibration process, not only the material parameters, but the particle size needs to be taken into consideration.
- The numerical tool is able to capture with sufficient accuracy the load against displacement behaviour obtained experimentally.
- The model can be used as a research tool to aid on the understanding of the processes related to the brittle failure of masonry.
- Reliable prediction of masonry strength can allow one to reduce the costly and timely experimental testing and avoid the usage of conservative empirical formulas.
- As the size of the elements increases, the run time for the execution of the results increases. In this instance, it may be beneficial that a compromise between size of voronoi element and accuracy of the model defined by the user.
- The computational time needed to execute the simulation is manageable. Using two Intel(R) Xeon(R) CPU @ 2.60GHz processors and 256 GB memory RAM, the time needed to perform the simulation was less than 10 minutes for the tensile and shear strength tests and a bit less than 30 minutes for the compressive strength tests.

Suggestions for future work involve the development of a systematic calibration procedure of micro-parameters and investigation on how such micro-parameters affect their related macro-parameters of the masonry constituents. In addition, further studies on masonry specimens containing irregular

surfaces and other small-scale experimental tests on masonry will be carried out and the suitability of the proposed approach to accurately simulate such mechanical behaviour of masonry will be further examined.

References

Atkinson, R. H., and Noland, J. L. A proposed failure theory for brick masonry in compression. Proc., 3rd Canadian Masonry Symp 1983., Edmonton, Alta., Canada, 5.1–5.17.

Azevedo N.M., Lemos J.V., Almeida J.R. Discrete element particle modelling of stone masonry. In: Sarhosis V., Lemos J.V., Bagi K., Milani G, ed. Computational Modelling of Masonry Structures Using the Discrete Element Method. IGI Global, 2016:146-169.

Berto L., Saetta A., Scotta R., Vitaliani R. An orthotropic damage model for masonry structures. Int J Numer Methods Eng 2002, 55, 127-157.

Castellazzi, G., D'Altri, A. M., de Miranda, S., Chiozzi, A., & Tralli, A. Numerical insights on the seismic behavior of a non-isolated historical masonry tower. Bulletin of Earthquake Engineering 2018, 16(2), 933–961.

Cruz T.V.G. & Pierce M.E. A 3DEC model for heavily veined massive rock masses, American Rock Mechanics Association. 48th US Rock Mechanics/Geomechanics Symposium held in Minneapolis 2014, MN, USA, 1-4 June.

Drysdale, R.G., Hamid, A. A., and Baker, L. R. Masonry structures: Behaviour and design, Prentice-Hall, Englewood Cliffs, N.J: 1994

Giambanco G., Rizzo S., Spallino R. (2001). Numerical Analysis of Masonry Structures via Interface Models, Computer Methods in Applied Mechanics and Engineering 190, 49-50, 6493–6511.

Heyman, J. Structural Analysis: A historical approach. University Press, Cambridge, UK: 1998.

Hendry, A.W. Structural Masonry. 2nd Edition, Macmillan Press, London: 1998.

Itasca. UDEC - Universal Distinct Element Code. Itasca Consulting Group, Minneapolis, MN, USA, 2014.

Kazerani T, Zhao J. Micro-mechanical parameters in bonded particle method for modelling of brittle material failure. International journal for numerical and analytical methods in geomechanics 2010;34:187-1895.

Lan H, Martin CD, Hu B. Effect of Heterogeneity of brittle rock on micromechanical extensile behaviour during compression loading. Journal of Geophysical Research 2010;115(1):1-14.

Lemos JV. Discrete Element Modeling of Masonry Structures, International Journal of Architectural Heritage 2007;1(2):190–213.

Lourenço PB, Rots JG. and Blaauwendraad J. Continuum Model for Masonry: Parameter Estimation and Validation, Journal of Structural Engineering 1998;124(6):642–652.

Lourenço PB & Rots JG. A multi-surface interface model for the analysis of masonry structures. Journal of Engineering Mechanics 1997;123(7):60-668.

Lourenço PB. *Computational strategies for masonry structures*, PhD thesis, Delft University of Technology, Delft, Netherlands, 1996.

Lourenço P.B. Computations on historic masonry structures. Progress in Structural Engineering and Materials 2002;4(3):301-319.

Milani G, Taliercio A. In-plane failure surfaces for masonry with joints of finite thickness estimated by a Method of Cells-type approach. Computers & Structures 2015;150:34-51.

Milani G, Taliercio A. Limit analysis of transversally loaded masonry walls using an innovative macroscopic strength criterion. International Journal of Solids and Structures 2016;81:274–293.

Mayya N, Rajan VT. An efficient shape representation scheme using Voronoi skeletons. Pattern Recognition Letters 1994;16: 147-160

Oliveira DV. Experimental and numerical analysis of blocky masonry structures under cyclic loading, PhD thesis, University of Minho, Portugal, 2003.

Pela L, Cerera M, Roca P. An orthotropic damage model for the analysis of masonry structures. Construction and Building Materials 2012;41:957-67.

Pina-Henriques J, & Lourenco PB. Masonry compression: A numerical investigate at the meso-level. Engineering Computational: International Journal for Computer-Aided Engineering and Software 2005;23(4):382-407.

Pluijm Van der R. Material properties of masonry and its components under tension and shear. In: Neis VV, editor. Canadian Masonry Symposium: Proceedings of the 6th Canadian Masonry Symposium 1992; Saskatoon, Saskatchewan, Canada; 675–86.

Pluijm Van der R. Shear behaviour of bed joints. In. Hanid AA, Harris HG, editors. North American Masonry Conference. In: Proceedings of the 6th North American Masonry Conference 1993; Philadelphia, Pennsylvania, USA, 25–36.

Potyondy D, Cundall PA. A bonded-particle model for rock. International Journal Rock Mechanics and Mining Science 2004;41(8):1329-1364.

Radnić J, Harapin A, Smilović M, Grgić N, Glibić M. Static and dynamic analysis of the old stone bridge in Mostar. Građevinar 2012;64 (8):655-665.

Roca P, Cervera M, Gariup G, Pela L. Structural Analysis of Masonry Historical Constructions. Classical and Advanced Approaches. Arch Comput Methods Eng 2010;17: 299–325.

Sarhosis V. Micro-modelling options for masonry structures. In: Sarhosis V., Lemos J.V., Bagi K., Milani G, ed. Computational Modelling of Masonry Structures Using the Discrete Element Method. IGI Global. 2016.

Sarhosis V, Oliveira DV, Lourenco PB. On the mechanical behaviour of masonry structures. In: Sarhosis V., Bagi K., Lemos J.V., Milani G, ed. Computational Modelling of Masonry Structures Using the Discrete Element Method. USA: IGI Global, 2016a.

Sarhosis V, Bagi K, Lemos JV, Milani G. Computational modeling of masonry structures using the discrete element method. USA: IGI Global, 2016b.

Sarhosis V. Computational modelling of low bond strength masonry. Phd thesis, University of Leeds, UK: 2012.

Smoljanović H, Živaljić N, Nikolić Ž. A combined finite-discrete element analysis of dry stone masonry structures, Engineering Structures 2013;52:89-100.